



Cite this: *RSC Adv.*, 2017, 7, 1418

# One-step immobilization of antibodies on ZIF-8/ Fe<sub>3</sub>O<sub>4</sub> hybrid nanoparticles for the immunoassay of *Staphylococcus aureus*

Changyong Yim,† Hyeonjeong Lee,† Sanghee Lee and Sangmin Jeon\*

Zeolitic imidazolate framework-8 (ZIF-8)-coated Fe<sub>3</sub>O<sub>4</sub> magnetic nanoparticle clusters (MNCs) were synthesized and used to detect pathogenic bacteria in milk. Hydrothermally synthesized MNCs were encapsulated with ZIF-8 *via* sonochemical reactions. Half fragments of monoclonal *Staphylococcus aureus* antibodies were conjugated to the low-coordinated Zn sites located on the outer layer of ZIF-8 *via* Zn–S bonding, which allows one-step immobilization of antibodies with favorable orientations on ZIF-8. Furthermore, ZIF-8 encapsulation improved the stability of MNCs in water by suppressing the Fe<sub>3</sub>O<sub>4</sub> oxidation. After the capture and magnetic separation of *Staphylococcus aureus* in milk using hybrid nanoparticles, bacteria concentration was determined with a portable ATP luminometer and the detection limit was found to be 300 cfu mL<sup>-1</sup>.

Received 20th October 2016  
Accepted 23rd November 2016

DOI: 10.1039/c6ra25527b

www.rsc.org/advances

## Introduction

Fe<sub>3</sub>O<sub>4</sub> magnetic nanoparticles have recently attracted considerable attention in bio-applications owing to their inherent superparamagnetic properties and biocompatibility.<sup>1–3</sup> The functionalization of antibodies on the Fe<sub>3</sub>O<sub>4</sub> nanoparticles enables the selective capture and magnetic separation of target molecules such as DNA,<sup>4</sup> biomarker proteins,<sup>5,6</sup> and pathogens<sup>7</sup> from complex sample solutions. The efficiency of magnetic separation increases with the size of the Fe<sub>3</sub>O<sub>4</sub> particles. However, clusters of small Fe<sub>3</sub>O<sub>4</sub> nanoparticles are preferred to large individual nanoparticles for immunomagnetic assays because Fe<sub>3</sub>O<sub>4</sub> assumes ferromagnetic properties at sizes larger than 30 nm.<sup>8</sup>

Despite the several advantages of Fe<sub>3</sub>O<sub>4</sub> magnetic nanoparticles for bio-applications, their use is hindered by the fact that Fe<sub>3</sub>O<sub>4</sub> undergoes oxidation in water, which affects the magnetic properties and appearance of the nanoparticles. To prevent the oxidation of Fe<sub>3</sub>O<sub>4</sub>, iron oxide particles are encapsulated with protective layers such as silicon dioxide (SiO<sub>2</sub>).<sup>9–11</sup> However, encapsulation with silica requires the careful control of reaction conditions for avoiding particle aggregation and decreases the saturation magnetization value of the encapsulated magnetic particles due to the high density of SiO<sub>2</sub> (2.195 g cm<sup>-3</sup>).<sup>12</sup> Furthermore, the antibodies immobilized on silica-coated magnetic nanoparticles *via* silane chemistry generally

possesses random orientations, which degrades the binding efficiency of the antibodies to target molecules.<sup>13</sup>

To overcome these drawbacks of silica encapsulation, we coated magnetic nanoparticle clusters (MNCs) with metal-organic frameworks (MOFs). Owing to their large surface areas, exceptional chemical and thermal stabilities, and negligible cytotoxicity, MOFs have been widely applied in drug delivery,<sup>14</sup> biomineralization,<sup>15</sup> and biomolecule purification.<sup>5</sup> Among the various MOFs, zeolitic imidazolate framework-8 (ZIF-8) was used in this study because it can be synthesized within 10 min without inducing nanoparticle aggregation and is chemically and thermally stable.<sup>16</sup> In addition, the low density of ZIF-8 (0.35 g cm<sup>-3</sup>) does not significantly decrease the saturation magnetization value of the hybrid MNCs. Furthermore, the low-coordinated Zn sites located on the outer shell of ZIF-8 could form Zn–S bonds,<sup>17–19</sup> which allows conjugation with thiolated antibodies and offers an attractive functionalization route for ZIF.

In this study, we synthesized ZIF-8-coated hybrid magnetic nanoparticle clusters (ZIF-8/MNCs) and functionalized them with half fragments of monoclonal *Staphylococcus aureus* (*S. aureus*) antibodies *via* Zn–S bonding, which enabled one-step immobilization of antibodies with favorable orientations. *S. aureus* is enterotoxigenic bacteria found in various foods such as milk and cheese. Milk was selected as a real food matrix to confirm that ZIF-8/MNCs can detect *S. aureus* in the presence of various interferents. After the capture and magnetic separation of *S. aureus* in milk using the hybrid nanoparticles, the concentration of bacteria was determined with a portable ATP luminometer. The detection limit of the assay was found to be 300 cfu mL<sup>-1</sup>. In addition, it was found that the ZIF coating improved the stability of MNCs in water by

Department of Chemical Engineering, Pohang University of Science and Technology (POSTECH), Pohang, Gyeongbuk 37673, Republic of Korea. E-mail: jeons@postech.ac.kr

† These authors contributed equally.



suppressing  $\text{Fe}_3\text{O}_4$  oxidation. To the best of our knowledge, this study reports the first approach for the direct functionalization of antibodies on ZIF-8/MNCs and their applications in immunomagnetic assays.

## Experimental

### Materials

Iron(III) chloride hexahydrate ( $\text{FeCl}_3 \cdot 6\text{H}_2\text{O}$ ), sodium citrate, urea, polyacrylamide (PAM;  $M_w = 5\,000\,000\text{--}6\,000\,000\text{ g mol}^{-1}$ ), zinc nitrate hexahydrate ( $\text{Zn}(\text{NO}_3)_2 \cdot 6\text{H}_2\text{O}$ ), 2-methylimidazole (2-MIM), potassium dihydrogen phosphate ( $\text{H}_2\text{KPO}_4$ ), potassium phosphate dibasic ( $\text{HK}_2\text{PO}_4$ ), tris(2-carboxyethyl)-phosphine (TCEP), Tween 20, lysogeny broth (LB) and methanol were purchased from Sigma-Aldrich (St. Louis, MO) and used without further purification. A monoclonal *S. aureus* antibody was purchased from Abcam (Cambridge, UK), and casein hydrolysate was purchased from MP Biomedicals (Santa Ana, CA, USA). Deionized (DI) water (18.3 M $\Omega$  cm) was obtained from a reverse osmosis water system (Human Science, Korea).  $\text{H}_2\text{KPO}_4$  (0.272 g) and  $\text{HK}_2\text{PO}_4$  (1.714 g) were dissolved in 1 L of DI water to prepare a phosphate buffer (PB) with pH = 7.4.

### Synthesis of $\text{Fe}_3\text{O}_4$ magnetic nanoparticle clusters (MNCs)

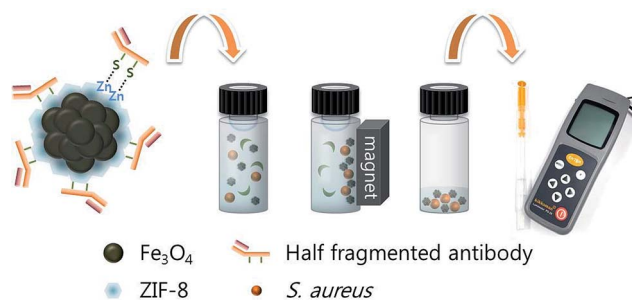
$\text{Fe}_3\text{O}_4$  was synthesized using a one-pot hydrothermal method described elsewhere.<sup>20</sup> Briefly, 2.16 g of  $\text{FeCl}_3 \cdot 6\text{H}_2\text{O}$ , 4.7 g of sodium citrate, and 1.44 g of urea were dissolved in 30 mL of DI water and 30 mL of 0.02 g  $\text{mL}^{-1}$  PAM solution in DI water was then added to the solution. The mixture was transferred to a 100 mL Teflon-lined stainless-steel autoclave and maintained at 200 °C in an oven for 12 h. After the autoclave was cooled to room temperature (RT), the black precipitate was collected using a permanent magnet and washed several times with DI water and ethanol. The resulting MNCs were dried in an oven at 90 °C for 12 h under reduced pressure.

### Synthesis and oxidation stability test of ZIF-8-coated hybrid MNCs (ZIF-8/MNCs)

The ZIF encapsulation reaction was conducted under sonication at 60 °C for 10 min by adding 0.1 g of  $\text{Fe}_3\text{O}_4$  MNCs to a 30 mL methanol solution containing 0.238 g of  $\text{Zn}(\text{NO}_3)_2 \cdot 6\text{H}_2\text{O}$ , 0.657 g of 2-MIM, and 10  $\mu\text{L}$  of HCl. The hybrid ZIF-8/MNCs were then collected using a permanent magnet and washed several times with methanol. The hybrid nanoparticles were dried in a vacuum oven at 90 °C for 12 h. For the oxidation stability test of ZIF-8/MNCs, they were kept in DI water at 200 °C for 1 h and variations in light absorption were measured using a UV-Vis spectrometer (UV-1800, SHIMADZU).

### Direct immobilization of half-fragmented antibody on ZIF-8/MNCs

10  $\mu\text{L}$  of 1.4 mg  $\text{mL}^{-1}$  TCEP in PB was added to 400  $\mu\text{L}$  of PB containing 10  $\mu\text{g}$  of monoclonal *S. aureus* antibody and incubated for 1 h at RT to reduce the disulfide bonds between the heavy and light chains of the antibody.<sup>21</sup> After purification



Scheme 1 Detection of *Staphylococcus aureus* using antibody-conjugated ZIF-8/MNCs and a portable ATP luminometer.

using Amicon centrifugal 10k filters (Millipore, Ireland), the half-fragmented antibodies were added to 1.5 mg of ZIF-8/MNC in PB for 1 h at RT to immobilize *via* Zn-S bonding. This one-step antibody conjugation using the half-fragmented antibodies eliminates the use of linker molecules and results in the immobilization of the antibodies with favorable orientations. The antibody-conjugated MNCs were sequentially incubated with 0.7 wt% casein and 0.1 wt% Tween 20 to prevent nonspecific binding and rinsed several times with PB.

### Detection of *Staphylococcus aureus* in milk using antibody-conjugated ZIF-8/MNC

Scheme 1 shows the experimental procedure for detecting pathogenic bacteria. Half fragments of monoclonal *S. aureus* antibody were immobilized onto ZIF-8/MNCs. A pure culture of *S. aureus* was grown in LB at 37 °C overnight, and the concentration of *S. aureus* was determined by cell counting on an agar plate. Subsequently, the culture solution was serially diluted into milk to obtain  $10^2$  to  $10^5$  cfu  $\text{mL}^{-1}$ . Diluted solutions (10 mL) were incubated with 0.1 mg of antibody-conjugated ZIF-8/MNCs for 1 h at RT. The bacteria were magnetically separated and dispersed in 100  $\mu\text{L}$  PB and mixed with benzalkonium chloride solutions for the lysis and ATP extraction of bacteria. Lysate solutions were sequentially added to lyophilized luciferase and luciferin powder, and the luminescence intensity from oxidized luciferin was measured by a portable luminometer (Kikkoman PD-20).<sup>22,23</sup>

## Results and discussion

Fig. 1(a) and (b) show a scanning electron microscopy (SEM) image and transmission electron microscopy (TEM) image of the MNCs, respectively. The average diameter of the MNCs was measured to be  $\sim 300$  nm. The SEM and TEM images of the ZIF-8/MNCs are shown in Fig. 1(c) and (d), respectively. The thickness of the ZIF-8 shell was  $\sim 80$  nm. The crystal structures of the MNCs and ZIF-8/MNCs were investigated using X-ray diffraction (XRD; Fig. 1(e)). The magnetite phase was observed in the MNCs at  $18.1^\circ$ ,  $29.7^\circ$ ,  $35.0^\circ$ ,  $42.5^\circ$ ,  $52.7^\circ$ , and  $56.3^\circ$ , which correspond to the (111), (220), (311), (400), (422), and (511) planes, respectively (indexed by JCPDC 890951). The



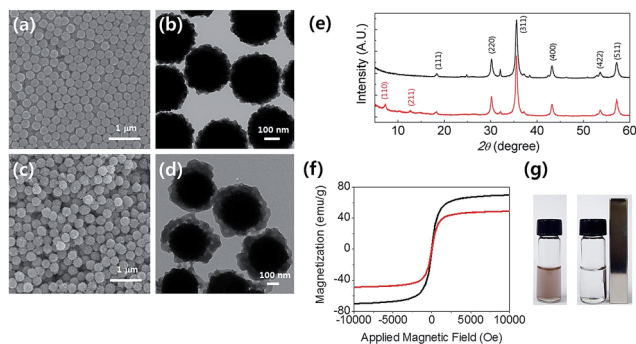


**Fig. 1** Characterization of MNCs and ZIF-8/MNCs: (a) SEM and (b) TEM images of MNCs; (c) SEM and (d) TEM images of ZIF-8/MNCs; (e) XRD patterns of MNCs (black) and ZIF-8/MNCs (red); and (f) magnetization curves of MNCs (black) and ZIF-8/MNCs (red). (g) Optical images of ZIF-8/MNCs in DI water before (left) and after (right) magnetic separation for 30 s.

XRD pattern of ZIF-8 on MNCs showed peaks at  $7.31^\circ$  and  $12.71^\circ$ , which correspond to the (110) and (211) planes of ZIF-8, according to CCDC 602542. Both the TEM and XRD results of the ZIF-8/MNCs indicated that the ZIF-8 shell was successfully coated onto the MNCs. Fig. 1(f) shows that both the MNCs and ZIF-8/MNCs exhibited superparamagnetic properties with saturation magnetizations of 70 and  $49 \text{ emu g}^{-1}$ , respectively.

Because of the low density of ZIF-8, the encapsulation of the MNCs with an  $\sim 80 \text{ nm}$ -thick layer of ZIF-8 decreased the saturation magnetization value only by 30%. If the MNCs were covered by a layer of  $\text{SiO}_2$  with the same thickness, the saturation magnetization would decrease by 70%. Fig. 1(g) shows that nearly complete magnetic separation was achieved within 30 s using a permanent magnet. Both the nanoparticles were well re-dispersed after the permanent magnet was removed.

To assess the degree of oxidation of  $\text{Fe}_3\text{O}_4$  in water, MNCs and ZIF-8/MNCs were kept in DI water at  $200^\circ\text{C}$  for 1 h.  $\text{Fe}_3\text{O}_4$  is known to be oxidized to maghemite ( $\gamma\text{-Fe}_2\text{O}_3$ ) at this moderate temperature and to hematite ( $\alpha\text{-Fe}_2\text{O}_3$ ) at higher temperatures ( $>500^\circ\text{C}$ ).<sup>24,25</sup> Although the saturation magnetization value of maghemite is not considerably different from that of  $\text{Fe}_3\text{O}_4$ ,<sup>24,25</sup> their different appearances often mislead people to conclude that the properties have been changed. Fig. 2(a) and (b) show optical images of MNCs and ZIF-8/MNCs, respectively, before and after heat treatment. The MNC solution changed from dark brown to pale yellow brown after heat treatment, whereas negligible changes in color were observed for the ZIF-8/MNC solution. Fig. 2(c) shows variations in the light absorption spectra of MNCs and ZIF-8 MNCs after heat treatment. Whereas a substantial change in the absorption peak wavelength was observed for MNCs, a negligible change was observed for ZIF-8/MNCs. This indicates that the ZIF-8 layers prevented the oxidation of  $\text{Fe}_3\text{O}_4$  due to their hydrophobic pore structures.<sup>26</sup>

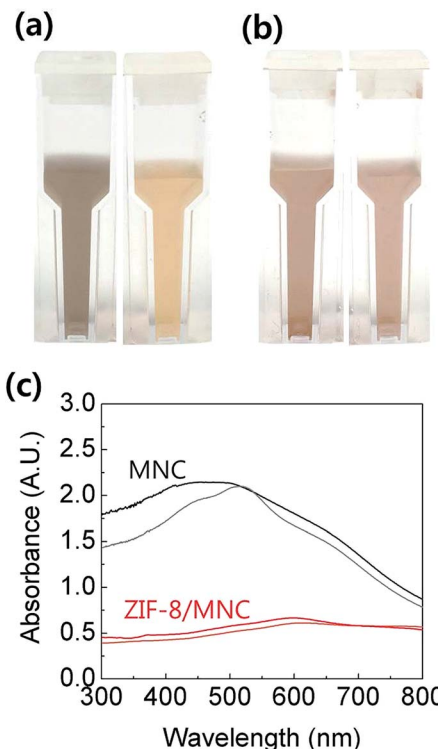


**Fig. 2** (a) Optical images of as-synthesized MNCs before (left) and after (right) heat treatment at  $200^\circ\text{C}$  for 1 h. (b) Optical images of as-synthesized ZIF-8/MNCs before (left) and after (right) heat treatment at  $200^\circ\text{C}$  for 1 h. (c) Variations in UV-VIS spectrum of as-synthesized MNCs (black: before heat treatment, gray: after heat treatment) and ZIF-8/MNCs (red: before heat treatment, orange: after heat treatment) in water.

The sensitivity of the assay was investigated using milk solutions spiked with various concentrations of *S. aureus*. Antibody-functionalized ZIF-8/MNCs were added to 10 mL of milk that had been spiked with  $0\text{--}10^5 \text{ cfu mL}^{-1}$  of *S. aureus*. After incubation at RT for 1 h, the bacteria were magnetically separated and rinsed several times with PB. Fig. 3(a) shows a TEM image of a ZIF-8/MNC-bound *S. aureus* bacterium. The bacterial surface was covered by ZIF-8/MNCs, indicating the effective capture of target bacteria using ZIF-8/MNCs. The ATP luminescence was measured using a portable ATP luminometer. The luminescence intensities were increased with increasing concentration of *S. aureus*. The detection limit for the *S. aureus*-spiked milk solution was found to be  $300 \text{ cfu mL}^{-1}$  as shown in Fig. 3(b).

The selectivity of the assay was examined using control experiments with milk solutions spiked with  $10^5 \text{ cfu mL}^{-1}$  *Escherichia coli*, *Salmonella typhimurium*, *Vibrio parahaemolyticus*, and *Listeria monocytogenes*. *S. aureus*-antibody-conjugated ZIF-8/MNCs were used to capture the bacteria in each solution, and the ATP luminescence was measured. Fig. 4 shows that the intensity of the ATP luminescence measured in the control experiments was very weak, indicating that nonspecific binding was negligible.



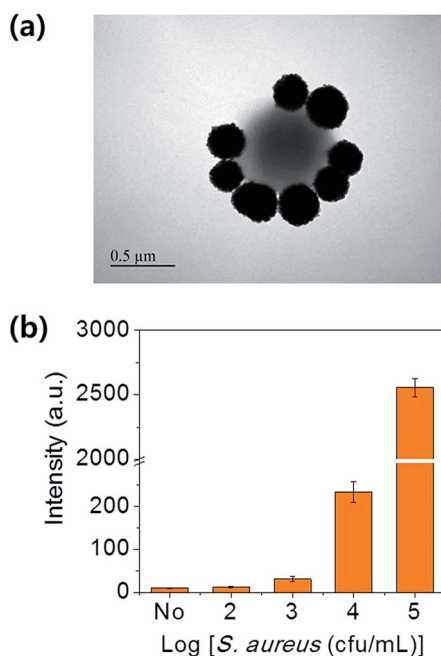


Fig. 3 (a) TEM image of a ZIF-8/MNC-bound *S. aureus* bacterium. (b) Intensities of ATP luminescence measured from a milk solution spiked with different concentrations of *S. aureus*.

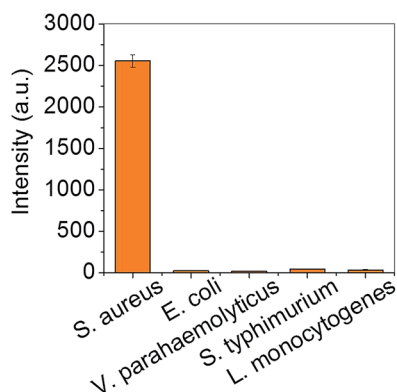


Fig. 4 Intensities of ATP luminescence measured from milk solutions spiked with different bacteria at concentrations of  $10^5$  cfu mL<sup>-1</sup>.

## Conclusions

In summary, we synthesized ZIF-8-coated MNCs and used them to detect pathogenic bacteria in milk. The low-coordinated Zn sites located on the outer layer of ZIF-8 offer binding sites for thiolated antibodies; also, half-fragmented antibodies could be directly conjugated on the ZIF-8/MNCs without linker molecules. After the capture and magnetic separation of *S. aureus* in milk using the hybrid ZIF-8/MNCs, the concentration of bacteria was determined using a portable ATP luminometer. The detection limit was 300 cfu mL<sup>-1</sup>. Furthermore, ZIF encapsulation was found to improve the stability of MNCs in water by suppressing the oxidation of Fe<sub>3</sub>O<sub>4</sub>, which facilitates the application of the hybrid particles for the on-site detection of pathogenic bacteria.

## Acknowledgements

This research was supported by the National Research Foundation of Korea (NRF) funded by the Korea government (MEST) (NRF-2014R1A2A2A01007027).

## References

- 1 S. Laurent, D. Forge, M. Port, A. Roch, C. Robic, L. Vander Elst and R. N. Muller, *Chem. Rev.*, 2008, **108**, 2064–2110.
- 2 J. B. Mamani, A. J. Costa-Filho, D. R. Cornejo, E. D. Vieira and L. F. Gamarra, *Mater. Charact.*, 2013, **81**, 28–36.
- 3 S. Adarsh, H. Hiroshi and A. Masanori, *Nanotechnology*, 2010, **21**, 442001.
- 4 D. Dressman, H. Yan, G. Traverso, K. W. Kinzler and B. Vogelstein, *Proc. Natl. Acad. Sci. U. S. A.*, 2003, **100**, 8817–8822.
- 5 J. Zheng, Z. Lin, G. Lin, H. Yang and L. Zhang, *J. Mater. Chem. B*, 2015, **3**, 2185–2191.
- 6 C. Chun, J. Joo, D. Kwon, C. S. Kim, H. J. Cha, M.-S. Chung and S. Jeon, *Chem. Commun.*, 2011, **47**, 11047–11049.
- 7 D. Kwon, S. Lee, M. M. Ahn, I. S. Kang, K.-H. Park and S. Jeon, *Anal. Chim. Acta*, 2015, **883**, 61–66.
- 8 H. Deng, X. Li, Q. Peng, X. Wang, J. Chen and Y. Li, *Angew. Chem., Int. Ed.*, 2005, **44**, 2782–2785.
- 9 H. L. Ding, Y. X. Zhang, S. Wang, J. M. Xu, S. C. Xu and G. H. Li, *Chem. Mater.*, 2012, **24**, 4572–4580.
- 10 Y. Deng, D. Qi, C. Deng, X. Zhang and D. Zhao, *J. Am. Chem. Soc.*, 2008, **130**, 28–29.
- 11 P. Jung-Nam, Z. Peng, H. Yong-Sheng and W. M. Eric, *Nanotechnology*, 2010, **21**, 225708.
- 12 C. Hui, C. Shen, J. Tian, L. Bao, H. Ding, C. Li, Y. Tian, X. Shi and H.-J. Gao, *Nanoscale*, 2011, **3**, 701–705.
- 13 Q. Weiping, X. Bin, W. Lei, W. Chunxiao, S. Zengdong, Y. Danfeng, L. Zuhong and W. Yu, *J. Inclusion Phenom. Macrocylic Chem.*, 1999, **35**, 419–429.
- 14 J. Zhuang, C.-H. Kuo, L.-Y. Chou, D.-Y. Liu, E. Weerapana and C.-K. Tsung, *ACS Nano*, 2014, **8**, 2812–2819.
- 15 K. Liang, R. Ricco, C. M. Doherty, M. J. Styles, S. Bell, N. Kirby, S. Mudie, D. Haylock, A. J. Hill, C. J. Doonan and P. Falcaro, *Nat. Commun.*, 2015, **6**, 7240.
- 16 Y. Pan, Y. Liu, G. Zeng, L. Zhao and Z. Lai, *Chem. Commun.*, 2011, **47**, 2071–2073.
- 17 F. Ke, L.-G. Qiu, Y.-P. Yuan, F.-M. Peng, X. Jiang, A.-J. Xie, Y.-H. Shen and J.-F. Zhu, *J. Hazard. Mater.*, 2011, **196**, 36–43.
- 18 S. Wang, Y. Fan and X. Jia, *Chem. Eng. J.*, 2014, **256**, 14–22.
- 19 L. Chang-Moon, J. DooRye, C. Su-Jin, K. Eun-Mi, J. Min-Hee, K. Sun-Hee, K. Dong Wook, L. Seok Tae, S. Myung-Hee and J. Hwan-Jeong, *Nanotechnology*, 2010, **21**, 285102.
- 20 W. Cheng, K. Tang, Y. Qi, J. Sheng and Z. Liu, *J. Mater. Chem.*, 2010, **20**, 1799–1805.
- 21 H. Sharma and R. Mutharasan, *Anal. Chem.*, 2013, **85**, 2472–2477.
- 22 K. Ito, K. Nishimura, S. Murakami, H. Arakawa and M. Maeda, *Anal. Chim. Acta*, 2000, **421**, 113–120.
- 23 W. Lee, D. Kwon, B. Chung, G. Y. Jung, A. Au, A. Folch and S. Jeon, *Anal. Chem.*, 2014, **86**, 6683–6688.





- 24 K. Haneda and A. H. Morrish, *J. Phys. Colloques*, 1977, **38**, 321–323.
- 25 M. I. Dar and S. A. Shivashankar, *RSC Adv.*, 2014, **4**, 4105–4113.
- 26 K. Zhang, R. P. Lively, C. Zhang, W. J. Koros and R. R. Chance, *J. Phys. Chem. C*, 2013, **117**, 7214–7225.

